# Quantitative Cherenkov emission spectroscopy for tissue oxygenation assessment

Axelsson, Johan; Glaser, Adam K.; Gladstone, David J.; Pogue, Brian W.

*Published in:*
Optics Express

*DOI:*
10.1364/OE.20.005133

2012

# Quantitative Cherenkov emission spectroscopy for tissue oxygenation assessment

**Johan Axelsson,[1,4,5] Adam K. Glaser,[1] David J. Gladstone,[2] and Brian W. Pogue[1,2,3,*]**

[1]*Thayer School of Engineering, Dartmouth College, Hanover, New Hampshire 03755, USA*
[2]*Norris Cotton Cancer Center, Dartmouth-Hitchcock Medical Center, Lebanon, New Hampshire 03766, USA*
[3]*Department of Physics and Astronomy, Dartmouth College, Hanover, New Hampshire 03755, USA*
[4]*Current address: Lund University, Department of Physics, Lund, Sweden*
[5]*johan.axelsson@fysik.lth.se*
[*]*brian.w.pogue@dartmouth.edu*

**Abstract:** Measurements of Cherenkov emission in tissue during radiation therapy are shown to enable estimation of hemoglobin oxygen saturation non-invasively, through spectral fitting of the spontaneous emissions from the treated tissue. Tissue oxygenation plays a critical role in the efficacy of radiation therapy to kill tumor tissue. Yet in-vivo measurement of this has remained elusive in routine use because of the complexity of oxygen measurement techniques. There is a spectrally broad emission of Cherenkov light that is induced during the time of irradiation, and as this travels through tissue from the point of the radiation deposition, the tissue absorption and scatter impart spectral changes. These changes can be quantified by diffuse spectral fitting of the signal. Thus Cherenkov emission spectroscopy is demonstrated for the first time quantitatively in vitro and qualitatively in vivo, and has potential for real-time online tracking of tissue oxygen during radiation therapy when fully characterized and developed.



**OCIS codes:** (170.1470) Blood or tissue constituent monitoring; (170.3660) Light propagation in tissues; (170.6510) Spectroscopy, tissue diagnostics; (170.6280) Spectroscopy, fluorescence and luminescence.

## References and links

1. J. Axelsson, S. C. Davis, D. J. Gladstone, and B. W. Pogue, "Cerenkov emission induced by external beam radiation stimulates molecular fluorescence," Med. Phys. **38**(7), 4127–4132 (2011).
2. M. A. Lewis, V. D. Kodibagkar, O. K. Oz, and R. P. Mason, "On the potential for molecular imaging with Cerenkov luminescence," Opt. Lett. **35**(23), 3889–3891 (2010).
3. H. Liu, G. Ren, Z. Miao, X. Zhang, X. Tang, P. Han, S. S. Gambhir, Z. Cheng, "Molecular optical imaging with radioactive probes," PLoS ONE **5**(3), e9470 (2010).
4. R. Robertson, M. S. Germanos, C. Li, G. S. Mitchell, S. R. Cherry, and M. D. Silva, "Optical imaging of Cerenkov light generation from positron-emitting radiotracers," Phys. Med. Biol. **54**(16), N355–N365 (2009).
5. A. E. Spinelli, D. D'Ambrosio, L. Calderan, M. Marengo, A. Sbarbati, and F. Boschi, "Cerenkov radiation allows in vivo optical imaging of positron emitting radiotracers," Phys. Med. Biol. **55**(2), 483–495 (2010).
6. J. V. Jelley, *Cerenkov radiation and its applications* (Pergamon Press, 1958).
7. L. H. Gray, A. D. Conger, M. Ebert, S. Hornsey, and O. C. Scott, "The concentration of oxygen dissolved in tissues at the time of irradiation as a factor in radiotherapy," Br. J. Radiol. **26**(312), 638–648 (1953).
8. P. Vaupel, A. Mayer, and M. Höckel, "Relationship between hemoglobin levels and tumor oxygenation," in *Recombinant Human Erythropoietin (rhEPO) in Clinical Oncology*, M. R. Nowrousian, ed. (Springer, 2008), pp. 265–282.
9. S. M. Evans and C. J. Koch, "Prognostic significance of tumor oxygenation in humans," Cancer Lett. **195**(1), 1–16 (2003).
10. M. Nordsmark, S. M. Bentzen, V. Rudat, D. Brizel, E. Lartigau, P. Stadler, A. Becker, M. Adam, M. Molls, J. Dunst, D. J. Terris, and J. Overgaard, "Prognostic value of tumor oxygenation in 397 head and neck tumors after primary radiation therapy. An international multi-center study," Radiother. Oncol. **77**(1), 18–24 (2005).
11. R. A. Cooper, C. M. L. West, J. P. Logue, S. E. Davidson, A. Miller, S. Roberts, I. J. Statford, D. J. Honess, and R. D. Hunter, "Changes in oxygenation during radiotherapy in carcinoma of the cervix," International Journal of Radiation. Oncology*. Biology*, Physics **45**, 119–126 (1999).

#158358 - $15.00 USD Received 21 Nov 2011; revised 9 Jan 2012; accepted 10 Jan 2012; published 16 Feb 2012

12. K. Vishwanath, D. Klein, K. Chang, T. Schroeder, M. W. Dewhirst, and N. Ramanujam, "Quantitative optical spectroscopy can identify long-term local tumor control in irradiated murine head and neck xenografts," J. Biomed. Opt. **14**(5), 054051 (2009).
13. S. H. Law, N. Suchowerska, D. R. McKenzie, S. C. Fleming, and T. Lin, "Transmission of Cerenkoverenkov radiation in optical fibers," Opt. Lett. **32**(10), 1205–1207 (2007).
14. P. Cherenkov, "Visible Emission of Clean Liquids by Action of $\gamma$ Radiation," Dokl. Akad. Nauk SSSR **2**, 451–454 (1934).
15. H. H. Ross, "Measurement of b-emitting nuclides using Cherenkov radiation," Anal. Chem. **41**(10), 1260–1265 (1969).
16. I. E. Tamm and I. M. Frank, "Coherent radiation from a fast electron in a medium," Dokl. Akad. Nauk SSSR **14**, 107–112 (1937).
17. E. Podgorsak, *Radiation Oncology Physics: A Handbook for Teachers and Students*, (IAEA, 2005), http://www.iaea.org/books (2005).
18. NIST, "ESTAR: Stopping power and range tables for electrons," URL *http://physics.nist.gov/PhysRefData/Star/Text/ESTAR.html* (2011).
19. H. J. van Staveren, C. J. M. Moes, J. van Marie, S. A. Prahl, and M. J. C. van Gemert, "Light scattering in Intralipid-10% in the wavelength range of 400-1100 nm," Appl. Opt. **30**(31), 4507–4514 (1991).
20. G. Alexandrakis, F. R. Rannou, and A. F. Chatziioannou, "Tomographic bioluminescence imaging by use of a combined optical-PET (OPET) system: a computer simulation feasibility study," Phys. Med. Biol. **50**(17), 4225–4241 (2005).
21. S. A. Prahl, "Optical absorption of hemoglobin," URL *http://omlc.ogi.edu/spectra/hemoglobin/index.html* (2009).
22. G. M. Hale and M. R. Querry, "Optical constants of water in the 200-nm to 200-um wavelength region," Appl. Opt. **12**(3), 555–563 (1973).
23. H. Dehghani, M. E. Eames, P. K. Yalavarthy, S. C. Davis, S. Srinivasan, C. M. Carpenter, B. W. Pogue, and K. D. Paulsen, "Near infrared optical tomography using NIRFAST: Algorithm for numerical model and image reconstruction," Commun. Numer. Methods Eng. **25**(6), 711–732 (2009).
24. S. Srinivasan, B. W. Pogue, S. D. Jiang, H. Dehghani, and K. D. Paulsen, "Spectrally constrained chromophore and scattering near-infrared tomography provides quantitative and robust reconstruction," Appl. Opt. **44**(10), 1858–1869 (2005).
25. C. Baudelet and B. Gallez, "Effect of anesthesia on the signal intensity in tumors using BOLD-MRI: comparison with flow measurements by Laser Doppler flowmetry and oxygen measurements by luminescence-based probes," Magn. Reson. Imaging **22**(7), 905–912 (2004).
26. J. W. Severinghaus, "Simple, accurate equations for human blood O2 dissociation computations," J. Appl. Physiol. **46**(3), 599–602 (1979).
27. K. S. Chao, W. R. Bosch, S. Mutic, J. S. Lewis, F. Dehdashti, M. A. Mintun, J. F. Dempsey, C. A. Perez, J. A. Purdy, and M. J. Welch, "A novel approach to overcome hypoxic tumor resistance: Cu-ATSM-guided intensity-modulated radiation therapy," Int. J. Radiat. Oncol. Biol. Phys. **49**(4), 1171–1182 (2001).
28. K. Newbold, M. Partridge, G. Cook, S. A. Sohaib, E. Charles-Edwards, P. Rhys-Evans, K. Harrington, and C. Nutting, "Advanced imaging applied to radiotherapy planning in head and neck cancer: a clinical review," Br. J. Radiol. **79**(943), 554–561 (2006).

## 1. Introduction

Recently it was demonstrated that Cherenkov emission is induced by MeV photons or electrons from a linear accelerator and detectable using a CMOS camera [1]. In particular, the blue-dominated spectral emission could excite an embedded fluorophore such as protoporphyrin IX which is known to be present at increased levels in tumors. The optical Cherenkov signal is induced when highly energetic charged particles travel through a dispersive medium like tissue. Based on this origin of contrast several reports have also shown the ability to image radioisotopes in vitro as well as in vivo [2–5]. Although optical Cherenkov emission is strongest in the blue, the broad band characteristics is well known with an intensity spectrum proportional to $\sim 1/\lambda^3$, or the number of photons per wavelength is proportional to $\sim 1/\lambda^2$ [6]. As this light propagates through tissue it will be affected by the oxygenated and deoxygenated hemoglobin as well as other chromophores. The difference in absorption between the hemoglobin chromophores is routinely used in NIR spectroscopy for tissue oxygenation assessments.

Tissue oxygenation plays a critical role in the efficacy of radiation therapy to kill tumor tissue [7]. Inadequate oxygen supply in tumor tissue (i.e. hypoxic areas) may lead to treatment failure through insufficient DNA damage in the tumor [8], and several clinical and pre-

#158358 - $15.00 USD Received 21 Nov 2011; revised 9 Jan 2012; accepted 10 Jan 2012; published 16 Feb 2012

clinical studies have shown that oxygenation monitoring is a prognostic factor in radiation therapy [8, 9]. Multi-center clinical studies have shown that pre-treatment tissue oxygen pressure ($pO_2$) is predictive of outcome in head and neck cancers [10], and other studies have shown that the $pO_2$ increases during the course of fractionated external beam radiation therapy [11], and that this change is correlated to effective local control. Optical hemoglobin spectroscopy has been used in-vivo, to show that oxygen hemoglobin saturation increases during fractionated radiation therapy in a rodent tumor model [12].

In this work, we show how oxygen saturation spectroscopy is achieved in-vivo and noninvasively, simply by measurement and spectral fitting of the endogenously emitted Cherenkov emission signal, as altered by absorption as it leaves the tissue or origin. A method is presented that relies on the spectral fitting of a theoretical light transport model to the Cherenkov emission spectrum. This study is the first presentation of this spectral signature, and will be followed by quantitative validation in further animal studies. By quantifying the absorption of the emitted photons coming from tissue chromophores, the hemoglobin oxygen saturation can be estimated. This is the first spectroscopic application of Cherenkov emission spectroscopy (CES) providing real-time physiological information about the tissue undergoing external beam radiation therapy.

## 2. Materials and methods

### *2.1 External beam radiation and experimental setup*

All experiments were performed with a linear accelerator (Varian Clinac 2100C, Varian Medical Systems, Palo Alto, USA). A circular beam shape with 30 mm diameter or a semi-circular beam shape with 24 mm diameter was used. Electron beams were used in all experiments with an approximate dose rate of 4Gy/min. The setup is shown schematically in Fig. 1(a). The fiber-bundle was positioned at 90° with respect to the external beam direction in order to minimize the Cherenkov emission induced directly in the fiber material [13]. Measurements of Cherenkov spectra were all taken while the radiation beam was directly hitting the phantoms or tissues.

### *2.2 Mathematical model of external beam induced Cherenkov emission*

Cherenkov emission is induced when electrons with a kinetic energy above 0.219 MeV propagate through a dispersive medium [14, 15]. The number of emitted Cherenkov photons, denoted $N(\lambda, E)$, within a spectral interval $[\lambda - \Delta\lambda, \lambda + \Delta\lambda]$ due to an electron with kinetic energy $E$ propagating a distance $dx$ is given by the Frank-Tamm formula [16], i.e.

$$dN(\lambda, E) = \frac{2\pi}{137}\left(\frac{1}{\lambda - \Delta\lambda} - \frac{1}{\lambda + \Delta\lambda}\right)\left(1 - \frac{1}{\beta(E)^2 n^2}\right)dx \tag{1}$$

In Eq. (1), $n$ is the refractive index of the medium, assumed to be 1.33 for water and 1.4 for soft tissue, and $\beta(E)$ is the velocity of the electron relative to the speed of light and its energy dependence is given by [15]

$$\beta(E) = \left[1 - \left(\frac{1}{\frac{E}{0.511} + 1}\right)^2\right]^{\frac{1}{2}} \tag{2}$$

The number of Cherenkov photons emitted within the spectral interval 400-700 nm is calculated using Eq. (1) and plotted in Fig. 1(b).

#158358 - $15.00 USD Received 21 Nov 2011; revised 9 Jan 2012; accepted 10 Jan 2012; published 16 Feb 2012

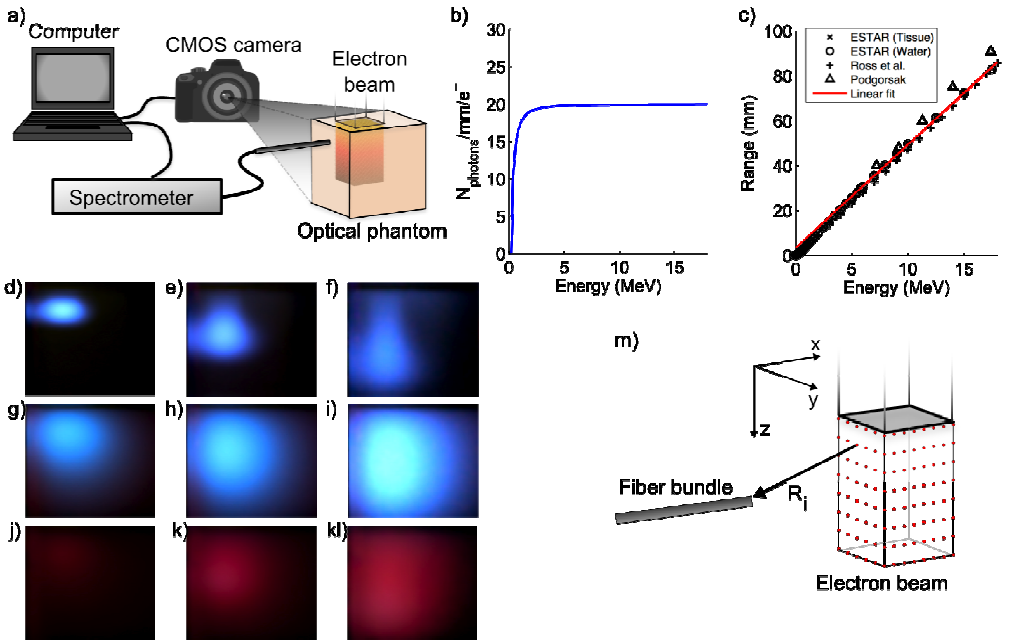


Fig. 1. Experimental setup. (a) a schematics showing the setup where electron beam irradiates from top of phantom. (b) the Frank-Tamm formula is plotted showing the number of photons generated per mm and electron for varying energy. (c) electron range as a function of energy. (d-f) electron beams at 6, 12 and 18 MeV irradiating a water tank. (g-i) electron beams irradiating a scattering solution of saline and intralipid. (j-l) electron beams irradiating a scattering phantom with added blood. (m) a schematic showing the optical point sources distributed throughout the electron beam.

As the electron propagates through the medium its kinetic energy will dissipate through inelastic collisions and according to the continuous slowing down approximation [17] the energy decreases linearly with depth. Assuming that an electron travels on a straight path from the surface given by the z-direction, the kinetic energy can be approximated by Harder's formula [17], i.e.

$$E = E_0\left(1-\frac{z}{R_p}\right). \tag{3}$$

Here $E_0$ (MeV) is the electron's incident energy at the surface and $R_p$ (mm) is the practical range of the electrons here given by

$$R_p = 4.612\times E_0 + 3.074. \tag{4}$$

Equation (4) is retrieved from a linear fit to several data sources i.e [15], [17]. and [18], specifying the most probable energy as a function of range. The data and linear fit is shown in Fig. 1(c).

Since the photon yield, in Eq. (1), is dependent on the energy and the energy decreases with depth, the number of emitted Cherenkov photons will change dependent on electron propagation distance. The depth dependent Cherenkov photon yield is then given by inserting Eq. (3) in Eq. (2) and defining

$$dN\left(\lambda, E_0, z\right) = \frac{2\pi}{137}\left(\frac{1}{\lambda-\Delta\lambda}-\frac{1}{\lambda+\Delta\lambda}\right)\left(1-\frac{1}{\beta\left(E_0,z\right)^2 n^2}\right)dx \tag{5}$$

#158358 - $15.00 USD Received 21 Nov 2011; revised 9 Jan 2012; accepted 10 Jan 2012; published 16 Feb 2012

where

$$\beta\left(E_0, z\right) = \left[1 - \left(\frac{1}{\frac{E_0}{0.511}\left(1 - \frac{z}{R_p}\right) + 1}\right)^2\right]^{\frac{1}{2}}. \quad (6)$$

The energy (and depth) dependence of the Cherenkov emission is demonstrated in the photographs in Fig. 1(d)-(f) where a water tank was irradiated from the top by 6, 12 and 18 MeV-electron beams.

During external beam radiation therapy, Cherenkov emission is generated in tissue hence the optical photons are subject to strong scattering and absorption. The effect of optical scattering on the Cherenkov emission is seen in Fig. 1(g)-(i) while the color-change seen in Fig. 1(j)-(l) indicates the presence of a spectrally dependent absorber, in this case 0.2% porcine blood added to the phantom. In this study we assume the simplest approach and adopt the Green's solution to the diffusion equation in order to describe the photon migration from the point of Cherenkov generation to the fiber bundle where the light is collected. However, as has been discussed above the Cherenkov emission is induced throughout the extent of the electron beam which is defined laterally by the beam shape and transversally by the electron range. Thus, absorption spectra of hemoglobin change the Cherenkov spectra, however the exact shape of the spectral distortion varies with beam profile and distance to the detecting fiber, as well as the expected variation with hemoglobin concentration and oxygenation.

To model this effect, Eq. (5) defines the number of photons emitted at a specific depth. In order to implement this in a forward numerical model, multiple point sources (~27000) are positioned within the coordinates that defines the beam, seen schematically in Fig. 1(m). The point source strength, or power, is given by Eq. (5), i.e. point sources placed deeper into the medium irradiate slightly weaker. At the detector position, the contributions from all the point sources are added. The detected intensity at one wavelength can then be evaluated by

$$I\left(\lambda\right) = C\sum_{i=1}^{M} \frac{hc}{\lambda} \frac{N\left(\lambda, E_0, z\right)}{4\pi D R_i} \exp\left(-\mu_{\text{eff}} R_i\right) \quad (7)$$

Where $D = \left(3\mu_s'\right)^{-1}$ and $\mu_{\text{eff}} = \sqrt{\mu_a / D}$ is the wavelength-dependent diffusion coefficient and effective attenuation coefficient respectively. The constant $C$ accounts for dose rate as well as conversion between fluence rate and detector intensity. The summation is performed for $M$ sources and the distance between each point source and the detector is given by $R_i$, also shown schematically in Fig. 1(m).

In order to retrieve a simulated Cherenkov emission spectrum Eq. (7) is evaluated for several wavelengths. For a given wavelength of interest, the waveband in Eq. (5) was chosen to be $\lambda \pm 0.5$ nm.

*2.3 Spectral fitting to retrieve chromophore concentrations*

The forward model presented above was used to extract the total hemoglobin concentration and hemoglobin oxygen saturation by a fitting procedure. The measured spectra and the calculated spectra were mean-normalized and compared within an iterative non-linear least squares method using Matlab 7.10.0 (The MathWorks Inc., Natick, Massachusetts, USA). Reduced scattering parameters were held constant within the fitting process and the wavelength dependent scattering was given by

$$\mu_s'(\lambda) = A\lambda^{-b} \quad (8)$$

#158358 - $15.00 USD Received 21 Nov 2011; revised 9 Jan 2012; accepted 10 Jan 2012; published 16 Feb 2012

where $A$ is the scatter amplitude, and $b$ is the scatter power. Scatter amplitude and power for the intralipid solutions were calculated from [19] while the mouse optical scattering parameters were compiled from [20]. The absorption coefficient was defined by

$$\mu_a(\lambda) = cHb_{tot} \times \left[ SO_2 \varepsilon_{HbO_2}(\lambda) + \left(1 - SO_2\right) \varepsilon_{Hb}(\lambda) \right] + C_w \mu_{H_2O}(\lambda) \tag{9}$$

where $cHb_{tot}$ is the total hemoglobin concentration, is the oxygen saturation while $\varepsilon_{HbO_2}$ and $\varepsilon_{Hb}$ is the extinction coefficient for oxy- and deoxy-hemoglobin respectively at wavelength λ [21]. $C_w$ is the water fraction, and $\mu_{H_2O}$ is the absorption coefficient of pure water at wavelength λ [22].

In each iteration $cHb_{tot}$ and $SO_2$ were updated before evaluating Eq. (7), and fitting for $SO_2$ in Eq. (9) based upon the full spectrum of wavelengths measured, fitted simultaneously. In the phantom experiments the method was calibrated using a scattering phantom with no absorber while fitting for $C_w$ only. This parameter was then fixed for the subsequent added blood experiments and the deoxygenation experiments. In the in vivo experiments calibration was performed using a euthanized animal assuming 0% oxygenation and 70% water fraction in the tissue.

Commonly oxygenation of tissue is estimated by the partial pressure of oxygen, $pO_2$, rather than SO2. The relationship between $pO_2$ and $SO_2$ is non-linear and described by the well known Hill saturation curve. While it is more informative to have direct measurement of pO2, it is largely recognized that direct measurement of this is challenging, due to the microscopic heterogeneity of $pO_2$ change with distance from capillaries. Bulk tissue $pO_2$ is thought to vary at least monotonically with bulk $SO_2$ when measured in tissue volumes greater than a millimeter cubed, although related non-linearly by the Hill curve. In this work, the tissue pO2 was not directly measured although it is known that tissue $pO_2$ and $SO_2$ are both near zero within minutes of animal euthanasia, and normal tissue hemoglobin $SO_2$ values can be in the range of 50-70% saturated.

*2.4 Phantom preparation*

The scattering liquid phantoms used in the experiments were made of phosphate buffered saline solution (D-PBS, Mediatech Inc, Manassas, VA), 0.2% v/v Intralipid© (Fresenius Kabi, Uppsala, Sweden) and porcine whole blood. Concentrations of 0.2% blood were used in most phantoms to mimic the expected concentration in murine skin. Prior to the experiments the hemoglobin concentration was measured using a hemoglobin meter (Hb 201 + , Hemocue, Ängelholm, Sweden). The oxygenation reference instrument was an ischemia monitoring system (Spectros T-stat, Spectros, Portola Valley, CA). Yeast was added in order to alter the oxygenation of the sample.

*2.5 Animal handling*

Four Balb/c mice were subject to external beam irradiation. Hair was removed by shaving the flanks of the animals. The mice were anesthetized with a ketamine/xylazine mixture administered intraperitoneally in a ratio of 90:10 mg/kg. Measurements were performed before and 30 min after the mice were euthanized through cervical dislocation.

*2.6 Spectrometer setup and data processing*

The spectrometer setup was governed by a spectrograph (Acton Insight, Princeton Instruments, Acton, USA) connected to a front illuminated CCD (Pixis 400F, Princeton Instruments, Acton, USA). The CCD was cooled to −70°C and the grating used in all experiments was 300 lines/mm. A 13 m long fiber bundle (Zlight, Latvia), composed of six 400 μm diameter silica fibers, collected the light at the phantom and guided the photons to the

#158358 - $15.00 USD Received 21 Nov 2011; revised 9 Jan 2012; accepted 10 Jan 2012; published 16 Feb 2012

spectrometer. The fiber bundle tip was positioned in contact with phantom boundary at the top surface of the liquid in the center of the beam. All spectra were acquired with an integration time of 60 seconds. Each spectrum was subject to background subtraction, normalization with integration time and binning by averaging four neighboring spectral bins. In all experiments the Cherenkov emission induced in the fiber was acquired before each experiment, and subtracted before data analysis.

### *2.7 Camera setup and image processing*

Images were acquired with a CMOS camera Nikon D90 (Nikon, Tokyo, Japan) equipped with a standard zoom lens Sigma EX 18-50/2.8 Macro HSM (Sigma Corporation, Kawasaki, Japan). The integration time for all images was 30 seconds. Images were processed by subtraction of a background image that was acquired in the same light conditions as when the beam irradiation was executed.

## 3. Results

### *3.1 Optical phantom experiments of hemoglobin concentration*

Phantoms, made of phosphate buffered saline solution (PBS), Intralipid© and porcine whole blood, were irradiated using a circular shaped electron beam at 18 MeV. The concentration of whole blood was changed and the spectra seen in Fig. 2(a) were obtained using the fiber-coupled spectrometer during beam irradiation. By fitting the forward model to each spectrum the total hemoglobin concentration was assessed and is shown in Fig. 2(b).

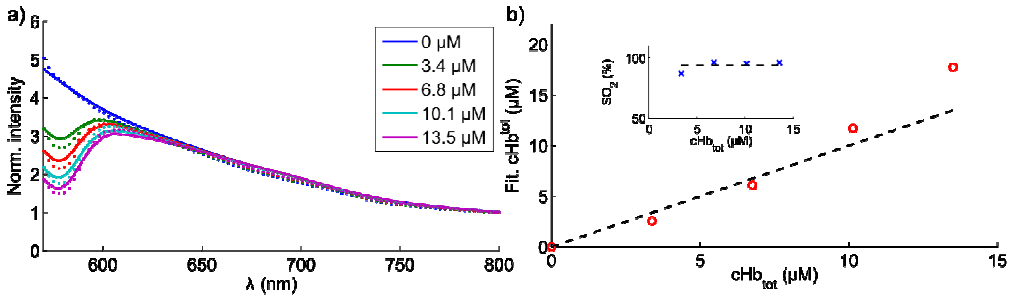


Fig. 2. Cherenkov emission spectroscopy of hemoglobin concentration. (a) Cherenkov emission spectra from phantom solutions with varying concentrations of porcine blood, indicated in the legend. (b) fitted values for the total hemoglobin concentration are offset against the true values. The inset shows the retrieved oxygenation values.

The absolute values for the measured hemoglobin concentrations are within 25% of the true concentrations. The inset in Fig. 2(b) shows the oxygen saturation, which on average is 93 +/– 4%. This value is in close agreement with the reference level of 92% that was acquired from the phantom using the ischemia monitoring system, see Materials and methods section.

In Fig. 2(a) it is seen that the predominant change in the spectrum as a function of blood concentration occurs at wavelengths shorter than approximately 630 nm.

### *3.2 Optical phantom experiments of oxygen saturation*

In order to investigate whether this technique is able to detect changes in tissue oxygenation, baking yeast was mixed into the scattering phantom containing blood. Measurements were acquired during beam irradiation before and approximately 30 minutes after adding the yeast.

#158358 - $15.00 USD Received 21 Nov 2011; revised 9 Jan 2012; accepted 10 Jan 2012; published 16 Feb 2012

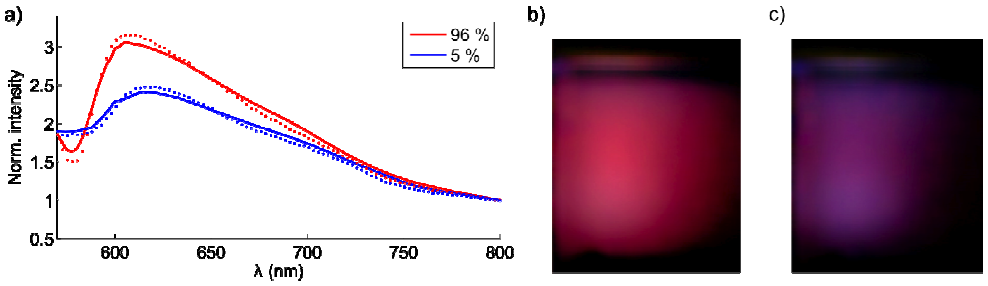


Fig. 3. Cherenkov emission spectroscopy of tissue oxygenation. (a) spectra from a well-oxygenated and a de-oxygenated scattering phantom solution are shown. The photos in (b) and (c) depict the color-change in the well- and de-oxygenated phantoms respectively.

The spectra are seen in Fig. 3(a). A change in hemoglobin oxygen saturation will change the spectral intensity and a shift towards blue wavelengths is expected. This is seen in the photographs from the oxygenated phantom in Fig. 3(b) and the de-oxygenated phantom in Fig. 3(c). By fitting the forward model to the two spectra, the retrieved tissue oxygenation was 96% in the well-oxygenated case and 5% in the de-oxygenated case. From previous experiments the ability to deoxygenate a solution with yeast has been confirmed multiple times, and is a standard way to induce nearly 0% oxygen saturation in the phantom.

*3.3 In vivo experiments of tissue oxygenation*

In order to demonstrate the method in-vivo, four healthy Balb/c mice were subject to external beam radiation on the hind flank. An electron beam at 18 MeV, shaped like a half-circle, irradiated the flank of the animal, see Fig. 4(a). Irradiation was performed before and after sacrifice, rendering one spectrum from oxygenated tissue and one spectrum from deoxygenated tissue.

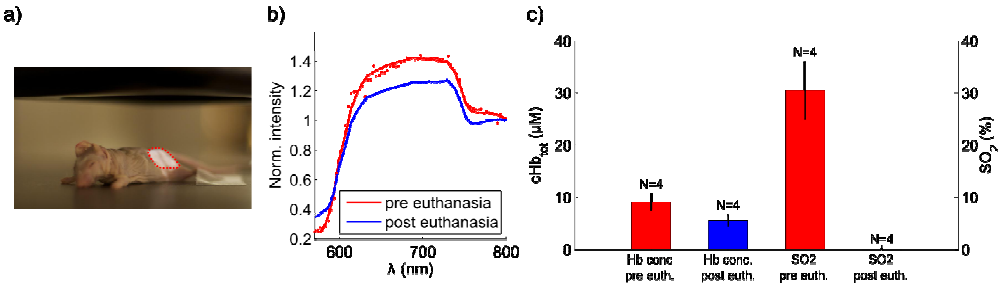


Fig. 4. Cherenkov emission spectroscopy of tissue oxygenation in vivo. (a) mouse positioned in the target region with the beam profile delineated in red. (b) typical spectra from a mouse pre and post euthanasia. (c) the results from the fitting procedure for both total hemoglobin concentration (left y-axis) and oxygen saturation (right y-axis). The mean of four animals is shown and the error bars indicate the standard deviation of this small population.

As with the phantom experiments the optical fiber was placed in the center of the beam. Typical spectra are seen in Fig. 4(b) and the results from the fitting procedure are stated in Fig. 4(c). As expected, after sacrifice, both the total hemoglobin concentration and consequently the oxygenation decrease. The differences in spectral shapes between the spectra from phantom experiments see Fig. 3(a), and in vivo experiments in Fig. 4(b) could be attributed to several factors. First, the scattering is most likely higher in the animal tissue than in the phantom solution making light from longer distances less likely to be detected. Secondly, the phantom geometry is large compared to the animal size allowing light to propagate throughout a larger volume. Thirdly, there might be other absorbers such as

#158358 - $15.00 USD Received 21 Nov 2011; revised 9 Jan 2012; accepted 10 Jan 2012; published 16 Feb 2012

melanin in the skin that perturb the spectral shapes. The in vivo results presented here are retrieved by calibrating the fitting procedure to a euthanized animal with assumed water content prior to the data evaluation. The SO2 values were 31% +/– 5% and 0% +/– 1% for normal respiration and after death, respectively. The hemoglobin values were 9 +/– 2 microMolar and 6 +/– 2 microMolar in the same two conditions. Clearly the hemoglobin values were slightly lower than might be expected and the SO2 during anesthesia might be lower than expected, although anesthesia with ketamine is known to reduce these values in vivo. Validation with external measurements was not available, however the changes expected before and after euthanasia were as expected here.

## 4. Discussion

The results presented in this work indicate that quantitative spectral analysis of Cherenkov light is possible for emission generated by high-energy external beam radiation. The phantom studies show that it is feasible to track changes of both total hemoglobin concentration and hemoglobin oxygen saturation. The range of concentrations of hemoglobin and intralipid where not chosen to be exhaustive here, but rather chosen to mimic the scattering and hemoglobin values expected in mouse skin. The in vivo study further demonstrates the applicability where a clear change between pre- and post- euthanasia of the mice was quantified using the method described here.

However, diffuse optical spectroscopy is non-unique meaning that several solutions exist to the inverse problem that satisfies the minimization criterion. This is a predicament arising from the fundamental property that light is diffusely scattered in tissue. Throughout this work the scattering properties of the medium under study, i.e. scattering amplitude and scattering power, have not been allowed to vary. In order to retrieve quantitative numbers for both chromophores and scattering properties, the spectral region needs to be optimized. A spectral interval at shorter wavelengths, e.g. between 480 and 650, seems to allow fitting of both chromophore concentrations and scattering parameters [12]. On the other hand shorter wavelengths make the method more sensitive to changes at shallow depths. In this work the fiber is placed in the beam since minimal Cherenkov emission was induced in the fiber if the angle between the beam and the fiber was 90°. However this setup makes the method mostly sensitive to changes in the tissue surface. In order to provide a more volumetric measure of the tissue oxygenation, more fibers are needed which could be easily added. The spectroscopic evaluation presented herein would in that case expand to a tomographic approach, see for example [23, 24]. Currently the optimal detector placement relative to the beam as well as optimal spectral interval to perform the data analysis is being investigated.

The in-vivo results retrieved from the mice, pre- and post-sacrifice, indicate low hemoglobin oxygen saturation. Normal mouse skin is thought to be fairly well oxygenated, with published estimates near 75% [20]. However, the mice were anesthetized with ketamine/xylazine, which suppresses blood flow as well as tissue oxygenation. It has been reported that anesthesia using ketamine/xyalzine results in a drop of about 50% of the $pO_2$ in a mouse leg muscle [25]. According to the oxygen dissociation curve a drop in $pO_2$ of 50% corresponds to a decrease in hemoglobin oxygen saturation from 75% to around 30% [26]. Hence, the lower oxygen saturation retrieved in-vivo is quite reasonable. Validation of the SO2 values and hemoglobin concentration was not possible at the time of this experiment, as specialized instrumentation would be required to do this, however the values observed are within plausible ranges of what could be expected in mouse skin tissue. Certainly the tissue phantom data was indicative of reasonable values for nearly fully oxygenated solutions and nearly fully deoxygenated solutions.

A low oxygen level in tumor tissue is a well-known prognostic marker for treatment failure of cancer and great efforts are dedicated to monitor and target these regions. PET imaging based on hypoxic markers [27, 28] can be used elegantly to reveal regions with oxygen deficiency using exogenous probes administered to the patient, but has had limited

#158358 - $15.00 USD Received 21 Nov 2011; revised 9 Jan 2012; accepted 10 Jan 2012; published 16 Feb 2012

clinical acceptance mostly due to cost. Cherenkov emission spectroscopy, as presented herein, will likely not be used for diagnosing hypoxic regions, unless within a few centimeters from the surface. However, the potential of the current method lies in treatment monitoring where changes in tissue oxygenation are of ample interest and are more accessible. The major benfit from Cherenkov light spectroscopy is the fact that the signal is inherently produced in all tissues being irradiated and requires no injectable contrast. However clearly the limitations are related to the penetration of the signal out of the volume being treated, or access by fiber optics to the region. Future work pursuing the idea of real-time evaluation of tissue oxygenation is warranted, and validation in tumor experiments with changes in tissue oxygen levels during fractionated therapy is planned based on this endogenous optical signal.

## 5. Conclusions

The demonstrated CES methodology provides the ability for quantitative analysis of hemoglobin concentration and oxygen saturation during external beam radiation therapy, as verified by tissue phantoms. The method utilizes the intrinsically generated Cherenkov radiation that is passively emitted from all tissue during radiation therapy. Preliminary in vivo testing has demonstrated that the values seen are plausible, and changes between living and dead tissue are as should be expected. This method has potential for tissue oxygenation monitoring during the course of standard fractionated radiation therapy treatments, thereby providing an easily implemented prognostic biomarker of the treatment efficacy. Further work must be done to quantitatively verify the estimation in vivo, using external correlates of tissue $SO_2$ and hemoglobin concentration, and this work is ongoing.

## Acknowledgments

This work has been funded by NIH grants RO1CA120368 and PO1CA084203. We gratefully acknowledge Luxi Xia for providing porcine whole blood for these experiments. We also would like to thank Julie O'Hara and Jason Gunn for their valuable help with animals.

#158358 - $15.00 USD Received 21 Nov 2011; revised 9 Jan 2012; accepted 10 Jan 2012; published 16 Feb 2012